

Black-hole mass estimates for a homogeneous sample of bright flat-spectrum radio quasars

G. Castignani^{1,*}, F. Haardt^{2,3}, A. Lapi^{4,1}, G. De Zotti^{5,1}, A. Celotti¹, and L. Danese¹

¹ SISSA, Via Bonomea 265, 34136, Trieste, Italy

² DiSAT, Università dell’Insubria, via Valleggio 11, I-22100 Como, Italy

³ INFN, Sezione di Milano Bicocca, Piazza Della Scienza 3, I-20126 Milano

⁴ Dipartimento di Fisica, Università ‘Tor Vergata’, Via della Ricerca Scientifica 1, I-00133 Roma, Italy

⁵ INAF-Osservatorio Astronomico di Padova, Vicolo dell’Osservatorio 5, I-35122 Padova, Italy

March 6th, 2013

ABSTRACT

We have selected a complete sample of flat-spectrum radio quasars (FSRQs) from the WMAP 7-yr catalog within the SDSS area, all with measured redshift, and have compared the black hole mass estimates based on fitting a standard accretion disk model to the ‘blue bump’ with those obtained from the commonly used single epoch virial method. The sample comprises 79 objects with a flux density limit of 1 Jy at 23 GHz, 54 of which (68%) have a clearly detected ‘blue bump’. Thirty-four of the latter have, in the literature, black hole mass estimates obtained with the virial method. The mass estimates obtained from the two methods are well correlated. If the calibration factor of the virial relation is set to $f = 4.5$, well within the range of recent estimates, the mean logarithmic ratio of the two mass estimates is equal to zero with a dispersion close to the estimated uncertainty of the virial method. The fact that the two independent methods agree so closely in spite of the potentially large uncertainties associated with each lends strong support to both of them. The distribution of black-hole masses for the 54 FSRQs in our sample with a well detected blue bump has a median value of $7.4 \times 10^8 M_{\odot}$. It declines at the low mass end, consistent with other indications that radio loud AGNs are generally associated with the most massive black holes, although the decline may be, at least partly, due to the source selection. The distribution drops above $\log(M_{\bullet}/M_{\odot}) = 9.4$, implying that ultra-massive black holes associated with FSRQs must be rare.

Key words. galaxies: active – quasar: general – black hole physics

1. Introduction

Reliable mass estimates of black-holes (BHs) in active galaxies are essential to investigate the physics of accretion and emission processes in the BH environment and the link between the BH growth and the evolution of galaxy stellar populations. However, getting them is not easy however. Dynamical mass estimates are only possible for nearby objects whose parsec-scale BH sphere of influence can be resolved, and are usually applicable to quiescent galaxies. BH masses of luminous active galactic nuclei (AGNs) are most commonly estimated using a technique known as ‘single epoch virial method’ or, briefly, ‘SE method’. Under the usual assumption that the broad-line region (BLR) is in virial equilibrium the BH mass is derived as

$$M_{\bullet} = f \frac{R_{\text{BLR}} \Delta V^2}{G}, \quad (1)$$

where R_{BLR} is the BLR radius, ΔV is the velocity of the BLR clouds (that can be inferred from the line width), f is the virial coefficient that depends on the geometry and kinematics of the BLR, and G is the gravitational constant. An effective way to estimate R_{BLR} , known as ‘reverberation mapping’, exploits the delay in the response of the BLR to short-term variability of the ionizing continuum (Blandford

& McKee 1982). The application of this technique has however been limited because it requires long-term monitoring of both the continuum and the broad emission lines. The SE method bypasses this problem exploiting the correlation between the size of the BLR and the AGN optical/UV continuum luminosity empirically found from reverberation mapping (Koratkar & Gaskell 1991; Kaspi et al. 2005; Bentz et al. 2009) and expected from the photo-ionization model predictions (Koratkar & Gaskell 1991). The AGN continuum luminosity can thus be used as a proxy for the BLR size.

However, measurements of the AGN continuum may be affected by various systematics: contributions from broad Fe II emission and/or from the host galaxy, and, in the case of blazars, contamination by synchrotron emission from the jet (Wu et al. 2004; Greene & Ho 2005). Fortunately, there are tight, almost linear correlations between the luminosity of the AGN continuum and the luminosity of emission lines such as $H\alpha$, $H\beta$, $Mg\ II$ and $C\ IV$ (Greene & Ho 2005; Vestergaard & Peterson 2006; Shen et al. 2011). It is thus expedient to estimate the BH masses using the line luminosities and full widths at half maximum (FWHMs).

Yet the reliability and accuracy of the method and of the resulting mass estimates, M_{\bullet} , is debated (Croom 2011; Assef et al. 2012). Each of its ingredients is endowed with a considerable uncertainty (Vestergaard & Peterson 2006;

* e-mail: castigna@sisssa.it

Park et al. 2012b). Recent estimates of the virial coefficient, f , differ by a factor $\simeq 2$. The luminosity-size relations have a significant scatter. In addition line-widths and luminosities vary on short timescales while black hole masses should not vary. These uncertainties are on top of those on the measurements of line-widths and luminosities, that need to be corrected for emissions from outside the BLR. Park et al. (2012b) found that uncertainties in the size–luminosity relation and in the virial coefficient translate in a factor $\simeq 3$ uncertainty in M_{\bullet} . But, as pointed out by Shen (2013), other sources of substantial systematic errors may also be present.

An independent method to estimate M_{\bullet} rests upon fitting the optical/UV ‘bump’ of AGNs (e.g. Malkan 1983; Wandel & Petrosian 1988; Laor 1990; Ghisellini et al. 2010; Calderone et al. 2013). In the the Shakura & Sunyaev (1973) accretion disk model the BH mass is a simple function of the frequency at which the disk emission peaks, which is a measure of the effective disk temperature, of the accretion rate, estimated by the disk luminosity, given the radiation efficiency and the inclination angle, i , i.e. the angle between the line-of-sight and the normal to the disk plane (Frank et al. 2002). However, this method had a limited application to estimate M_{\bullet} (Ferrarese & Ford 2005) mainly because reliable estimates of the intrinsic disk luminosity are very difficult to obtain. In fact: a) the inclination is generally unknown and the observed flux density is proportional to $\cos i$; b) the observed UV bump is highly sensitive to obscuration by dust either in the circum-nuclear torus or in the host galaxy; c) we need to subtract the contribution from the host galaxy that may be substantial particularly for the weaker active nuclei.

These difficulties are greatly eased in the case of flat-spectrum radio quasars (FSRQs) because: a) the accretion disk is expected to be perpendicular to the jet direction, and indeed there is good evidence that the jets of *Fermi* FSRQs are highly aligned (within 5°) with the line-of-sight (Ajello et al. 2012) so that $\cos i \simeq 1$; b) the obscuration is expected to be negligible because blazar host galaxies are thought to be passive, dust free, ellipticals (e.g. Giommi et al. 2012, and references therein) and also the torus is likely perpendicular to the line-of-sight; c) the contamination is also small because elliptical hosts are red, i.e. are faint in the UV. However, the UV emission may be contaminated by the emission from the relativistic jet.

On the other hand, the BH mass estimates obtained by fitting the blue bump rely on several assumptions whose validity is not fully proven (see Ghisellini et al. 2010, for a discussion): (i) the disk is described by a standard Shakura & Sunyaev (1973) model, i.e. the disk is optically thick and geometrically thin; (ii) the black hole is non-rotating, of Schwarzschild type; (iii) the SED is a combination of black body spectra. If any of these assumptions does not hold, the mass estimates would be affected. An additional uncertainty source in our practical application is that photometry of the SED beyond the peak is not always available. When it is available, it is not simultaneous with the optical data determining the rising part of the SED and needs corrections for extinction within our own galaxy and, in the case of objects at high- z , for photoelectric absorption in the intergalactic medium.

A cross-check of the outcome of the two, independent, approaches for FSRQs is therefore important to verify the reliability of the underlying assumptions of either method,

to estimate the associated uncertainties and to constrain the values of the parameters.

The plan of the paper is the following. The selection of the sample and the photometric data we have collected are presented in Section 2. In Section 3 we describe the components used to model the spectral energy distributions (SEDs) of our sources and the formalism to obtain the BH mass estimates from the ‘blue bump’ fitting. In Section 4 we briefly deal with estimates exploiting the SE method, found in the literature, compare them with our estimates, and present the distribution of BH masses obtained from the ‘blue bump’ fitting. Our main conclusions are summarized and briefly discussed in Section 5.

We adopt a standard flat Λ CDM cosmology with matter density $\Omega_m = 0.27$ and Hubble constant $H_0 = 71 \text{ km s}^{-1} \text{ Mpc}^{-1}$ (Hinshaw et al. 2009).

2. The sample

The Wilkinson Microwave Anisotropy Probe (WMAP) satellite has provided the first all-sky survey at high radio frequencies ($\geq 23 \text{ GHz}$). At these frequencies blazars are the dominant radio-source population. We have selected a complete blazar sample, flux-limited at 23 GHz (K band), drawn from the 7-year WMAP point source catalog (Gold et al. 2011).

The basic steps of our selection procedure are the following. We adopted a flux density limit of $S_K = 1 \text{ Jy}$, corresponding to the WMAP completeness limit (Planck Collaboration XIII 2011), and cross-matched the selected sources with the most recent version of the blazar catalogue BZCAT (Massaro et al. 2011)¹. This search yielded 248 catalogued blazars. To check whether there are additional bona-fide blazars among the other WMAP sources brighter than the adopted flux density limit we have collected data on them from the NASA/IPAC Extragalactic Database (NED)², from the database by Trushkin (2003) and from the catalog of the Australia Telescope Compact Array (ATCA) 20 GHz survey (AT20G, Hancock et al. 2011). Sources qualify as bona-fide blazars if they have: i) a flat radio spectrum ($F_{\nu} \propto \nu^{-\alpha}$ with $\alpha \leq 0.5$); ii) high variability; iii) compact radio morphology. Based on these criteria we have added to our blazar sample 7 sources that satisfy the first two criteria. The third criterion is satisfied by three of them, whereas for the others no radio image is available in the NED. Our initial sample then consists of 255 blazars, 243 of which have redshift measurements.

Since we are interested in characterizing the optical/UV bump attributed to the accretion disk we have restricted the sample to the 103 blazars within the area covered by the Eighth Data Release (DR8)³ of the Sloan Digital Sky Survey (SDSS), totalling over 14,000 square degrees of sky and providing simultaneous 5-band photometry with 95% completeness limiting AB magnitudes $u, g, r, i, z = 22.0, 22.2, 22.2, 21.3, 20.5$, respectively (Abazajian et al. 2004). With the exception of WMAP7 # 274 these objects are in the BZCAT. Moreover, since BL Lacs generally do not show the UV bump, we have dropped from our sample the 19 sources classified as BL Lacs, as well as the 5 sources classified as blazars of uncertain type, keeping only sources classified as

¹ www.asdc.asi.it/bzcat/

² ned.ipac.caltech.edu/

³ www.sdss3.org/dr8/

FSRQs. The final sample comprises 79 objects, all having spectroscopic redshift measurements.

2.1. Photometric data

For these 79 objects we have collected, updated and complemented the photometric data available on the NED, as described in the following.

2.1.1. SDSS DR8 data

SDSS counterparts of our FSRQs were searched adopting their low frequency radio coordinates which have uncertainties of $\simeq 1$ arcsec. Since the SDSS positional uncertainty adds very little to the error (the SDSS positional accuracy is of $\simeq 0.1$ arcsec) we have chosen a search radius of 3 arcsec. By construction, all our FSRQs have at least one SDSS counterpart within the search radius. In most cases we found a unique counterpart, with the SDSS photometry being consistent with extrapolations from data at nearby frequencies compliant with a type 1 QSO SED plus the jet emission. Only in eight cases (WMAP7 sources with id numbers 26, 30, 153, 182, 198, 250, 317, 353) we found multiple counterparts. However in each case one of the sources within the search radius was much (at least 2 magnitudes) brighter than the others, and had flux densities consistent with those of the FSRQ at nearby frequencies. Thus an unambiguous SDSS counterpart was found for all our FSRQs. They have a median and an average de-reddened AB r-band magnitude of 17.67 and 17.63 mag, with a rms dispersion of 1.31 mag. Thus they are generally much brighter than the 95% SDSS magnitude limit. Only one FSRQ in the sample, WMAP7 #314, has an r-band magnitude slightly fainter than that limit.

We have adopted the SDSS magnitudes corrected for Galactic extinction, as listed in the DR8 catalog and denoted e.g. as `dered_g`. As suggested in the DR8 tutorial⁴ we have decreased the DR8 u-band magnitudes by 0.04 to bring them to the AB system. The corrections to the magnitudes in the other bands are negligible. In principle some additional extinction may take place within the host galaxy, but we expect it to be negligible because the jet sweeps out any intervening material along its trajectory. The correction for absorption in the intergalactic medium (IGM) is described in sub-section 2.1.3. For the redshift range spanned by our sources it may be relevant only in the u and g bands.

The choice of the effective wavelength corresponding to each SDSS filter depends on the convolution of the filter spectral response function with the spectral shape of the source. We adopt the effective wavelengths reported in the SDSS tutorial⁵: 3543, 4770, 6231, 7625 and 9134 Å, for the u, g, r, i and z filters, respectively.

2.1.2. GALEX data

We have looked for UV photometry for our FSRQs in the sixth data release, GR6⁶, of the Galaxy Evolution Explorer (GALEX) satellite (Morrissey et al. 2007). GALEX provides near-UV (NUV, 1750–2800 Å) and far-UV (FUV,

1350–1750 Å) images down to a magnitude limit $AB \sim 20$ –21 with an estimated positional uncertainty of $\simeq 0.5$ arcsec. We adopt 1535 and 2301 Å as the effective wavelengths of the FUV and NUV filters, respectively.

Again the low frequency radio positions of FSRQs were used and a search radius of 3.5 arcsec was adopted. At least one counterpart was found for 65 objects. Multiple counterparts were found to correspond to GALEX measurements at different epochs of the same source (i.e. differences in coordinates were within the positional errors). Such multi-epoch measurements were found for 24 of our sources. In these cases we have adopted their weighted average. Whenever the $S/N < 3$, we have adopted upper limits equal to 3 times the error.

The UV fluxes are very sensitive to extinction within our Galaxy and, in the case of high- z objects, to photoelectric absorption in the intergalactic medium. To correct for Galactic extinction we have used the values of $E(B - V)$ given in the GR6 catalog for each source and the extinction curve by Cardelli et al. (1989), as updated by O’Donnell (1994), normalized to $A(V) = 3.1 E(B - V)$. The correction for absorption in the IGM is described in the next section.

2.1.3. Absorption in the intergalactic medium

Since we do not know the IGM attenuation along each line of sight we have used the effective optical depth $\tau_{\text{eff}}(z) = -\ln[\langle \exp(-\tau) \rangle]$, averaged over all possible lines of sight. We have computed, following Haardt & Madau (2012), $\tau_{\text{eff}}(z)$ at the effective wavelengths of SDSS u and g filters (the effective optical depth in the other 3 SDSS filters vanishes for the redshift range of interest here) and of the 2 GALEX filters. The results are shown in Fig. 1 and listed in Table 1. The step-like features are due to Lyman series absorption. We have verified that adopting the spectral response of each filter instead of considering the single effective wavelengths results in a small correction in the flux densities, and in the smoothing of all the edges in the optical depth as a function of redshift. Details on these calculations will be presented in a forthcoming paper (Madau & Haardt, in preparation).

2.1.4. X-ray data

We have found ROSAT data for 18 of the 79 FSRQs in our sample. However an inspection of the global SEDs indicates, for all of them, that X-ray data are clearly far from the fit of the blue bump in terms of a Shakura & Sunyaev (1973) accretion disk, adopted in this paper, and more likely related to other components such as the synchrotron or the inverse Compton ones or the emission from a bright hot X-ray corona.

2.1.5. WISE data

We have cross-correlated our FSRQs with the latest version of the Wide-field Infrared Survey Explorer (WISE; Wright et al. 2010) catalog⁷. Again, the coordinates of low radio frequency counterparts were adopted and a search radius of 6.5 arcsec was chosen, consistent with WISE positional

⁴ www.sdss3.org/dr8/algorithms/fluxcal.php#SDSStoAB

⁵ skyserver.sdss.org/dr1/en/proj/advanced/color/sdssfilters.asp

⁶ galex.stsci.edu/GR6/

⁷ wise2.ipac.caltech.edu/docs/release/allsky/

Table 1. Redshift dependent effective optical depth for IGM absorption, averaged over all lines of sight, at the effective wavelengths of the GALEX NUV and FUV bands and of SDSS the g and u bands.

z	$\tau_{\text{eff}}(1545)$	$\tau_{\text{eff}}(2267)$	$\tau_{\text{eff}}(3491)$	$\tau_{\text{eff}}(4884)$
0.271	0.000	0.000	0.000	0.000
0.333	0.030	0.000	0.000	0.000
0.399	0.030	0.000	0.000	0.000
0.468	0.030	0.000	0.000	0.000
0.540	0.042	0.000	0.000	0.000
0.615	0.049	0.000	0.000	0.000
0.695	0.063	0.000	0.000	0.000
0.778	0.146	0.000	0.000	0.000
0.865	0.232	0.000	0.000	0.000
0.957	0.320	0.047	0.000	0.000
1.053	0.412	0.047	0.000	0.000
1.154	0.506	0.047	0.000	0.000
1.370	0.706	0.076	0.000	0.000
1.487	0.812	0.098	0.000	0.000
1.609	0.926	0.233	0.000	0.000
1.737	1.052	0.384	0.000	0.000
1.871	1.193	0.551	0.000	0.000
2.013	1.352	0.737	0.112	0.000
2.160	1.530	0.943	0.112	0.000
2.316	1.729	1.173	0.112	0.000
2.479	1.951	1.428	0.184	0.000
2.649	2.199	1.712	0.230	0.000
2.829	2.475	2.026	0.330	0.000
3.017	2.782	2.376	0.808	0.000
3.214	3.124	2.764	1.338	0.404
3.421	3.506	3.207	1.924	0.404
3.638	3.930	3.713	2.573	0.404
3.866	4.402	4.280	3.291	0.673
4.105	4.927	4.915	4.086	0.842
4.356	5.511	5.626	4.964	1.195
4.619	6.158	6.424	5.936	2.581
4.895	6.875	7.317	7.010	4.110
5.184	7.669	8.318	8.196	5.794

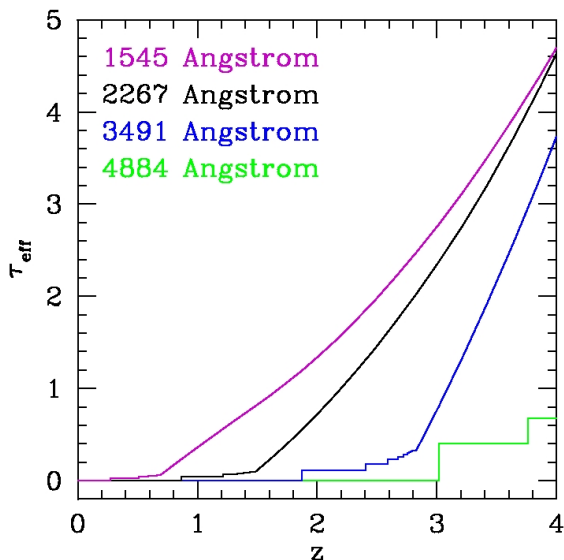


Fig. 1. Redshift dependent effective optical depth for IGM absorption, averaged over all lines of sight, at the effective wavelengths of SDSS g and u bands and of the GALEX NUV and FUV bands.

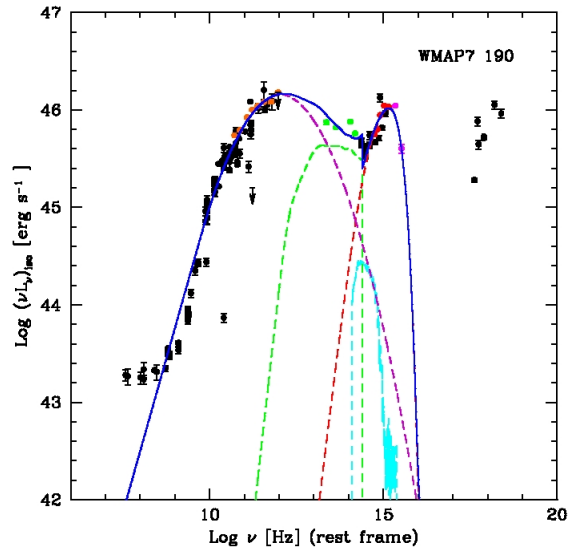


Fig. 2. Example of a SED fit (WMAP7 # 190). Solid blue parabola: total SED, which includes synchrotron emission, host galaxy, disk and torus emissions; dashed violet line: synchrotron from the jet; green dashed line: torus; dashed cyan line: host galaxy, taken to be a passive elliptical with $M_R = -23.7$; dashed red line: accretion disk. Orange points: Planck data; green: WISE data; red: SDSS data; magenta: GALEX data. Black points: data taken from the NASA/IPAC Extragalactic Database (NED). Note that, at variance with what was done to compute L_d (see text), the luminosities shown here are computed assuming isotropic emission.

uncertainty⁸. We found WISE counterparts with $S/N \geq 3$ in at least one band for all the 79 FSRQ in the sample. In the WISE bands where $S/N < 3$ we have adopted an upper limit equal to 3 times the error. Multiple WISE sources were found within the search radius for the FSRQs WMAP7 # 30, 126, 278, 317 and 378. In these cases we have chosen the brightest WISE source as the most likely counterpart. In all cases, the other sources were at least 2 magnitudes dimmer.

2.2. Planck data

In the *Planck* Early Release Compact Source Catalog (ERCSC; Planck Collaboration VII 2011) we have found counterparts for 72 out of our 79 FSRQs; 47, 39, and 68 of them have ERCSC flux densities at 70, 44, and 30 GHz, respectively and 63 have ERCSC flux densities at frequencies ≥ 100 GHz.

3. SED modeling

Of the 79 FSRQs in our sample, 54 (i.e. 68%) show clear evidence of the optical/UV bump, interpreted as the emission from a standard optically thick, geometrically thin accretion disk model (Shakura & Sunyaev 1973). As illustrated

⁸ According to the WISE Explanatory Supplement (Cutri et al. 2013), sources with $S/N \sim 20$ have a typical rms positional uncertainty of 0.43 arcsec. Our sources generally have a much lower S/N ratio and the astrometric uncertainty scales as $(S/N)^{-1}$ (e.g. Condon et al. 1998; Ivison et al. 2007). For the typical S/N values of our sources, $S/N = 3-5$, the search radius correspond to positional errors in the range $2.3-3.8\sigma$.

by the example shown in Fig. 2, the global SEDs are modeled taking into account several additional components: the Doppler boosted synchrotron continuum modeled following Donato et al. (2001); a passive elliptical host galaxy template (see, e.g., Giommi et al. 2012); the dusty AGN torus emission based on a type-1 QSO template (BQSO1) from the Polletta et al. (2007)⁹ SWIRE template library.

The fit of the global SED was made using 6 free parameters. Four are those of the blazar sequence model for the synchrotron emission (the 5 GHz luminosity, the 5 GHz spectral index, the junction frequency between the low- and the high-frequency synchrotron template and the peak frequency of νL_ν , Donato et al. 2001). The remaining two parameters refer to the accretion disk model (i.e. the normalization and the peak frequency). The other components are fixed. The host galaxy template is an elliptical (Mannucci et al. 2001) with an absolute magnitude of $M_R = -23.7$, as in Giommi et al. (2012). The normalization of the torus template was computed from that of the accretion disk emission, requiring that the torus/accretion disk luminosity ratio is equal to that of the Polletta et al. (2007) BQSO1 template.

We stress that accurate fits of the global SEDs are beyond the scope of the present paper whose main purpose is the estimate the black-hole masses by fitting the optical/UV bump with a Shakura & Sunyaev (1973) model, as discussed in the following. The consideration of the other components, fitted taking into account all the data we have collected, is mainly relevant to check whether they may contaminate the emission from the accretion disk. In many cases, the lack of simultaneity of the measurements does not allow reliable fits of the other components. Still for the 54 objects with clear evidence of the blue bump the data where enough either to estimate the amount of contamination or to signal points that should be better taken as upper limits to the blue bump emission.

The thermal emission from the accretion disk is modeled as a combination of black-bodies with temperatures depending on the distance, R , from the black-hole (see, e.g., Frank et al. 2002). The flux density observed at a frequency ν_o is given by:

$$F_\nu(\nu_o) = \nu_o^3 \frac{4\pi h_P \cos(i)}{c^2 D_A^2} \int_{R_\star}^{R_{\text{out}}} \frac{R dR}{e^{h_P(1+z)\nu_o/kT(R)} - 1}, \quad (2)$$

where D_A is the angular diameter distance to the blazar, k is the Boltzmann constant, z is the redshift of the source, h_P is the Planck constant, c is the speed of light, R_\star and R_{out} are the inner and outer disk radii, respectively. The radial temperature profile, $T(R)$, is given by:

$$T^4(R) = \frac{3GM_\bullet \dot{M}}{8\pi R^3 \sigma} \left(1 - \sqrt{\frac{R_\star}{R}}\right), \quad (3)$$

where G is the gravitational constant, M_\bullet is the black hole mass, \dot{M} is its accretion rate, σ is the Stefan-Boltzmann constant. R_\star is the radius of the last stable orbit that, for a Schwarzschild black hole, is $R_\star = 3R_S$, $R_S = 2GM_\bullet/c^2$ being the Schwarzschild radius. The results are insensitive to the chosen value for R_{out} provided that $R_{\text{out}} \gg R_\star$; we choose $R_{\text{out}} = 100R_S$.

⁹ [www.iasf-milano.inaf.it/~sim\\$polletta/templates/swire_templates.html](http://www.iasf-milano.inaf.it/~sim$polletta/templates/swire_templates.html)

Since the emission of the disk is anisotropic (the flux density measured by an observer is proportional to $\cos i$), the monochromatic luminosity is related to the flux density by (Calderone et al. 2013)

$$\nu_e L_\nu(\nu_e) = \frac{2\pi D_L^2 \nu_o F_\nu(\nu_o)}{\cos i}, \quad (4)$$

where $\nu_e = (1+z)\nu_o$ is the frequency at the emission redshift, z , and $D_L(z)$ is the luminosity distance.

For the 54 FSRQs showing the optical/UV bump the fit of the accretion disk model to it was done using only the SDSS (available for all of them) and the GALEX data (available for all but 7 of them). Using the standard minimum χ^2 technique we have obtained the values of the two free parameters, the normalization and the peak frequency, ν_{peak} (in terms of νL_ν). The total disk luminosity, L_d , can then be computed integrating eq. (4) over frequency. The derived values of $\nu_{\text{peak}} L_\nu(\nu_{\text{peak}})$, L_d and ν_{peak} are given in Table 2. The accretion rate is $\dot{M} = L_d/(\eta c^2)$ where η is the mass to light conversion efficiency for which we adopt the standard value $\eta = 0.1$.

An analysis of eq. (2) indicates that the main contribution to the integral comes from a region around the radius $R_{\text{peak}} = (49/36)R_\star$ where the temperature profile $T(R)$ [eq. (3)] reaches its maximum value T_{max} . The integral over R , to compute L_d (hence \dot{M}), can then be approximately evaluated with the steepest descent method. The calculation was made setting $i = 0$. Then, introducing the value of $T_{\text{max}} = T(R_{\text{peak}})$ in the Wien's displacement law, $\nu_{\text{peak}}/T_{\text{max}} \simeq 5.879 \times 10^{10} \text{ Hz K}^{-1}$, we get an estimate of the black hole mass: $M_\bullet/10^9 M_\odot \simeq 0.46(\nu_{\text{peak}}/3 \times 10^{15} \text{ Hz})^{-2}(\dot{M}/M_\odot \text{ yr}^{-1})^{1/2}$. This result shows that the estimate of M_\bullet is quite sensitive to the value of ν_{peak} . One may then wonder whether associating it to T_{max} is a sufficiently good approximation. To answer this question we have computed M_\bullet by numerically solving the equation $d \log(\nu_e L_\nu(\nu_e))/d \log(\nu_e) = 0$ for all values of ν_{peak} and L_d found for our sources. Remarkably, we find that the exact values of M_\bullet strictly follow the dependencies on \dot{M} and ν_{peak} given by the approximate solution, with a coefficient lower by a factor 0.76. The black hole masses implied by the Shakura & Sunyaev (1973) model can then be accurately computed using the simple equation:

$$\frac{M_\bullet}{10^9 M_\odot} \simeq 0.35 \left(\frac{\nu_{\text{peak}}}{3 \times 10^{15} \text{ Hz}} \right)^{-2} \left(\frac{\dot{M}}{M_\odot \text{ yr}^{-1}} \right)^{1/2}. \quad (5)$$

The results for our FSRQs are reported in Table 2.

The statistical errors associated with $\log(\nu_{\text{peak}})$ and \dot{M} were computed utilizing the standard criteria based on the χ^2 statistics (e.g., Cash 1976), with errors estimated adding in quadrature the measurement uncertainties and the estimated spread of data points due to variability. The uncertainty on $\log(\nu_{\text{peak}})$ was found to be in the range 0.02–0.09, that on $\log(\dot{M})$ in the range 0.02–0.10, depending on the data quality. The errors on $\log(M_\bullet)$ cannot be obtained by simply summing the two contributions in quadrature because $\log(\nu_{\text{peak}})$ and \dot{M} are not independent. From the distribution of $\log(M_\bullet)$ obtained varying the two quantities within their 68% confidence interval, we found uncertainties in the range 0.1–0.3.

The uncertainties on the IGM absorption correction due to variations of the effective optical depth with the line of sight are unknown. An insufficient correction for UV absorption leads to an underestimation of ν_{peak} and to an overestimation of M_{\bullet} , while an overcorrection has the opposite effect. However, since all of our FSRQs but one (namely WMAP7 # 137 that has a redshift $z = 3.4$) are at $z < 2.5$ the corrections for IGM absorption are relatively small. Ignoring such correction would lead to a mean overestimate of $\log(M_{\bullet})$ by 0.04 for the 18 objects with $z < 1$, of 0.09 for the 17 objects with $1 < z < 1.5$ and of 0.11 for the 13 objects at $1.5 < z < 2$. For WMAP7 # 137 and for the 5 objects at $2 < z < 2.5$ the variation of ν_{peak} is compensated by that of L_d so that the average difference between corrected and uncorrected estimates is negligible.

Further uncertainties are associated with the choice of the model and of its parameters. As pointed out in Sect. 1, the adopted accretion disk model assumes a non-rotating BH, although the chosen value of the radiation efficiency, $\eta = 0.1$, is above the maximum efficiency for a Schwarzschild BH. However, Calderone et al. (2013), using the Li et al. (2005) software package, found that the Shakura & Sunyaev (1973) model with $R_{\star} = 3R_S$, as used here, mimics quite well the SED for an optically thick, geometrically thin accretion disk around a Kerr BH with a spin parameter $a \simeq 0.7$, corresponding to a maximum radiative efficiency $\eta = 0.1$. For this choice of η our BH mass estimates are therefore little affected by having neglected the general relativistic effects associated with a Kerr BH. Based on the analysis presented in Appendix A4 of Calderone et al. (2013) we find for a pure Schwarzschild model ($a = 0$, $\eta = 0.06$) a BH mass lower by a factor of 0.6 while for a Kerr model with a maximum possible radiative efficiency ($a = 0.998$) we find a BH mass higher by a factor of 1.75. Note however that the latter factor is a generous upper limit since the boundaries of the range of values of η for which Shankar et al. (2009) achieved a good match to the overall shape of the BH mass function are $0.06 \leq \eta \leq 0.15$. The effect of the choice of the inclination angle i should be minor given the model and observational indications that $i \lesssim 5^\circ$; even if we double this value we get $\cos(10^\circ) = 0.985$.

Summing up in quadrature the uncertainties listed above we end up with errors on $\log(M_{\bullet})$ in the range 0.2–0.4. These estimates should be taken as lower limits since they do not include all the uncertainties in the theoretical accretion disk model, which are difficult to quantify.

4. Black hole mass estimates

4.1. Estimates with the single epoch virial method

Black hole mass estimates obtained with the single epoch virial method (SE method) are available in the literature for several FSRQs in our sample. Shaw et al. (2012) derived them for a sub-sample of blazars selected from the First Catalog of Active Galactic Nuclei detected by the Fermi Large Area Telescope (1LAC, Abdo et al. 2010), including 24 of our FSRQs. They considered several estimators exploiting continuum and emission line ($H\beta$, MgII, CIV) measurements. We preferred the estimates based on line measurements to those obtained by using the continuum luminosity because the latter is liable to contamination from the jet synchrotron emission. More precisely, we choose, in order of preference, estimates derived from $H\beta$ and MgII

lines for the blazars at redshift $z < 1$ and the ones derived from the MgII and CIV lines for the blazars at higher redshifts (see Shaw et al. 2012, for more details).

Shen et al. (2011) estimated the BH masses for a sample of quasars drawn from the SDSS-DR7 quasar catalog (Schneider et al. 2010), including 36 objects in common with our sample. Seventeen of the latter belong also to the Shaw et al. (2012) sample. However, although Shen et al. (2011) give measurements of line luminosities and FWHM, the fiducial BH masses reported by them are based on continuum rather than line luminosity. Thus we have used their line data to recompute the BH masses for the 36 objects in common with our sample. Since several line measurements are present for a given source, following Shen et al. (2011) we adopted $H\beta$, MgII, and CIV line measurements for the blazars at redshift $z < 0.7$, $0.7 \leq z < 1.9$, and $z \geq 1.9$, respectively. The average logarithmic ratio of the black hole mass estimates based on line luminosities to the fiducial values given by Shen et al. (2011), based on continuum luminosities, for the 36 sources is $\langle \log(M_{\bullet, \text{Shen, lines}}/M_{\bullet, \text{Shen}}) \rangle = -0.17$ with a rms dispersion of 0.23. This suggests that indeed the continuum luminosities are likely contaminated by the optical emission from the jet, as argued by Shen et al. (2011). Our re-evaluations of the BH mass estimates of the Shen et al. (2011) blazars are in good agreement with those by Shaw et al. (2012) for the 17 blazars in common. The average logarithmic ratio of the two estimates is $\langle \log(M_{\bullet, \text{Shaw}}/M_{\bullet, \text{Shen, lines}}) \rangle = 0.01$, with a dispersion of 0.22.

Since the analysis by Shaw et al. (2012) is focussed on FSRQs, for the comparison with the BH mass estimates obtained from the fitting of the blue bump we preferred their estimates for the objects in common with Shen et al. (2011). For the other Shen et al. (2011) blazars in our sample we have adopted our new determinations of BH masses based on line luminosities. The corresponding uncertainties were computed applying the standard error propagation, taking into account measurement errors on line luminosities and FWHMs as well as the errors on the coefficients of the relations between these quantities and the BH mass, as reported in Shen et al. (2011) and references therein. The latter errors are the main contributors to the global uncertainties.

Black hole mass estimates for one additional object in our sample, WMAP7 # 250, were reported by Kaspi et al. (2000) and Shang et al. (2007). We adopted the latter, more recent estimate.

4.2. The f -factor

The BH masses estimated with the SE method assume that the optical/UV line emission is coming mainly from the BLR, located at a radial distance R_{BLR} from the central black hole. Assuming that the BLR clouds are in virial equilibrium, M_{\bullet} is given by eq. (1). There are two commonly used measures of the cloud velocity ΔV : the line FWHM and the dispersion of its Gaussian fit. We adopt the second one, i.e. $\Delta V = \sigma_{\text{line}}$. R_{BLR} is estimated using empirical analytic relations with continuum or line luminosities. With these assumptions and notation for an isotropic velocity field we have $f = 3$ (Netzer 1990). This is however an over-simplified model. In practice, the value of f is empirically determined, but there is no consensus on its value (see Park et al. 2012a,b, and references therein).

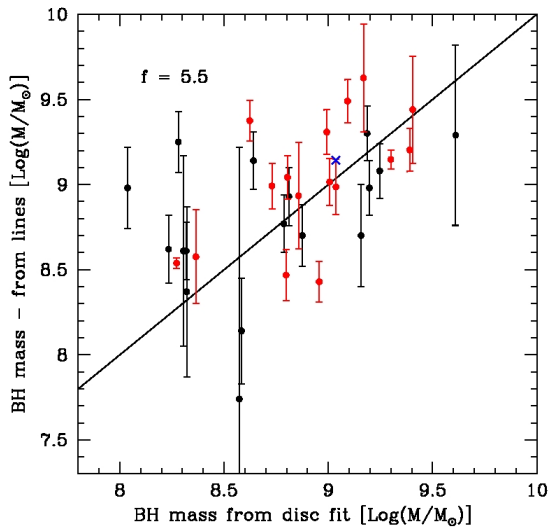


Fig. 3. Comparison of the black hole mass estimates. Estimates with the SE method against those from fitting the accretion disk SED. The black points are from Shaw et al. (2012), the red points are our estimates using line data from Shen et al. (2011), the blue cross refers to the estimate by Shang et al. (2007) corrected as mentioned in the text. No error was reported for this estimate.

Values claimed in the literature differ by a factor of 2, from $f \simeq 2.8$ (Graham et al. 2011) to $f \simeq 5.5$ (Onken et al. 2004). Note that for face-on objects (such as FSRQs) the average virial coefficient f may be larger than for optically selected QSOs (with random orientations) if the BLR has a flattened geometry (Decarli et al. 2011). The empirical relations used by Shen et al. (2011) and Shaw et al. (2012) implicitly assume $f = 5.5$ since this value was used, following Onken et al. (2004), in calibrating the reverberation mapping BH masses which in turn were used as standards to calibrate SE mass estimators. Shang et al. (2007) followed a different approach, adopting $f = 3$. The latter authors also used a slightly different cosmology. We have corrected their BH mass estimate to homogenize it with the others.

4.3. Comparison of black hole mass estimates

Thirty-four of the 54 blazars for which we could derive the BH masses with the blue bump fitting method also have published estimates with the SE method. In Figure 3 we compare the results from the two methods, after having homogenized the SE estimates as described above. They are well correlated: the Spearman test yields a 99.96% (i.e. 3.5σ) significance of the correlation. The SE method with $f = 5.5$ yields, on average, slightly higher values of M_{\bullet} . We find an average $\langle \log(M_{\bullet,SE}/M_{\bullet,blue\ bump}) \rangle = 0.09$ with a rms dispersion of 0.40 dex. For comparison, the uncertainty of the SE method is of 0.4–0.5 dex (Vestergaard & Peterson 2006; Park et al. 2012b) and that of the blue bump method is $\simeq 0.2$ –0.4 (see Sect. 3). Thus the rms difference is fully accounted for by the uncertainties of the two methods. The offset between the two estimates would be removed setting $f = 4.5$, well within the range of current estimates. However, in view of the large uncertainties, reading this as an estimate of f would constitute an over-interpretation of the

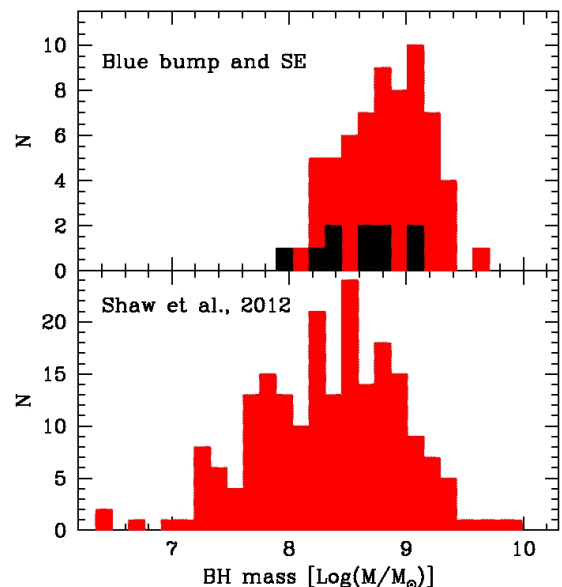


Fig. 4. Distributions of black hole masses. The upper panel shows in red the distribution for our 54 objects having estimates via blue bump fitting and, in black, for 10 additional objects in the sample for which we have BH mass estimates via the SE method only, homogenized as described in the text and decreased by 0.09 dex to remove the mean offset with blue bump estimates. The lower panel shows the distribution for all 1LAC blazars (Shaw et al. 2012) with masses decreased by 0.09 dex.

data. On the other hand, the consistency of the two methods strongly suggests that neither is badly off.

4.4. Distribution of black hole masses

In the upper panel of Fig. 4 we report in red the distribution of BH masses obtained by means of the blue bump fitting for 54 of our FSRQs and, in black, the distribution for the 10 additional ones for which only SE estimates are available. The estimates for the latter objects have been first homogenized as described above and then decreased by 0.09 dex to correct for the mean offset with the blue bump results. The lower panel shows, for comparison, the distribution for 1LAC blazars in the Shaw et al. (2012) sample, again decreasing the BH masses by 0.09 dex. Whenever Shaw et al. (2012) provide more than one mass estimate for a single object we made a choice abiding by the order of preference mentioned in Sect. 4.1.

The figure shows that our 64 FSRQs are associated with very massive BHs ($M_{\bullet} \gtrsim 10^{7.8} M_{\odot}$) with a median value of $6.8 \times 10^8 M_{\odot}$. The median BH mass changes little (it becomes $7.4 \times 10^8 M_{\odot}$) if we restrict ourselves to the 54 FSRQ with BH mass estimates via blue bump fitting. The decline of the distribution at lower masses may be a selection effect: we have selected radio-bright objects ($S_{23\text{GHz}} \geq 1 \text{ Jy}$) and the 15 (19%) FSRQs in our sample that do not show a detectable blue bump nor have SE estimates of the BH mass may well be associated with lower values of M_{\bullet} . On the other hand, our results are also consistent with the theoretical and observational studies which suggest that radio loud AGNs are generally associated with the most massive black holes ($M_{\bullet} \gtrsim 10^8 M_{\odot}$, e.g. Chiaberge & Marconi 2011). The fast decline of the distribution above $M_{\bullet} \simeq 10^{9.4} M_{\odot}$, sug-

gesting some upper bound to BH masses, is more likely to be real.

The BH mass distribution of Shaw et al. (2012) blazars adds support to the conclusion that *blazar* BH masses either below $M_{\bullet} \sim 10^{7.4} M_{\odot}$ or above $M_{\bullet} \sim 10^{9.6} M_{\odot}$ are rare. In this context it is worth noticing that errors in BH mass estimates tend to populate the tails of the distribution by an effect analogous to the Eddington bias: objects preferentially move from highly populated to less populated regions. Thus in particular the highest mass tail may be overpopulated (while the effect on the low mass tail may be swamped by selection effects).

In Figure 5 we report the distributions of the accretion rates (top panel) and of the Eddington ratios (bottom panel) for the 54 FSRQ in the sample for which we have estimated the BH mass fitting the blue bump of the spectrum, as reported in Table 2. We find a median Eddington ratio of 0.16 and a median accretion rate of $2.8 M_{\odot} \text{ yr}^{-1}$. The few extreme values of these parameters must be taken with special caution on account of the uncertainties affecting our estimates.

The BH mass turns out to be anti-correlated with the disk peak frequency. The Spearman’s test gives a probability of the null hypothesis (no correlation) $p = 6.8 \times 10^{-5}$. The anticorrelation follows from eq. (5) due to the weak dependence of M_{\bullet} on the accretion rate and the limited range of \dot{M} spanned by our blazars.

5. Discussion and conclusions

We have compared black hole mass estimates based on fitting the blue bump with a Shakura & Sunyaev (1973) model with those obtained with the commonly used single epoch virial method (SE method) for a complete sample of FSRQs drawn from the WMAP 7-yr catalog, all with measured spectroscopic redshift. The sample comprises 79 objects with $S_{23\text{GHz}} \geq 1 \text{ Jy}$, 54 of which (68%) have a clearly detected ‘blue bump’ from which the black hole mass could be inferred. FSRQs are the AGN population best suited for such a comparison because there is good evidence that their jets are highly aligned with the line-of-sight, suggesting that the accretion disk should be almost face-on, thus minimizing the uncertainty on the inclination angle that bewilders black hole mass estimates for the other AGN populations.

The mass estimates obtained from the two methods are well correlated. If the calibration factor f of the SE relation, eq. (1), is set $f = 4.5$, well within the range of recent estimates, the mean logarithmic ratio of the two mass estimates is $\langle \log(M_{\bullet, \text{SE}}/M_{\bullet, \text{blue bump}}) \rangle = 0$ and its dispersion is 0.40, close to that expected from uncertainties of the two methods. The fact that the two independent methods agree so closely in spite of all the potentially large uncertainties associated with each (see Sects. 1 and 3) lends strong support to both of them. However the agreement is only statistical, and individual estimates of black hole masses must be taken with caution.

The distribution of black-hole masses for the 54 FSRQs in our sample with a well detected blue bump has a median value of $7.4 \times 10^8 M_{\odot}$. It declines at the low mass end, consistent with other indications that radio loud AGNs are generally associated with the most massive black holes, although the decline may be, at least partly, due to the source selection. The distribution drops above $M_{\bullet} = 2.5 \times 10^9 M_{\odot}$,

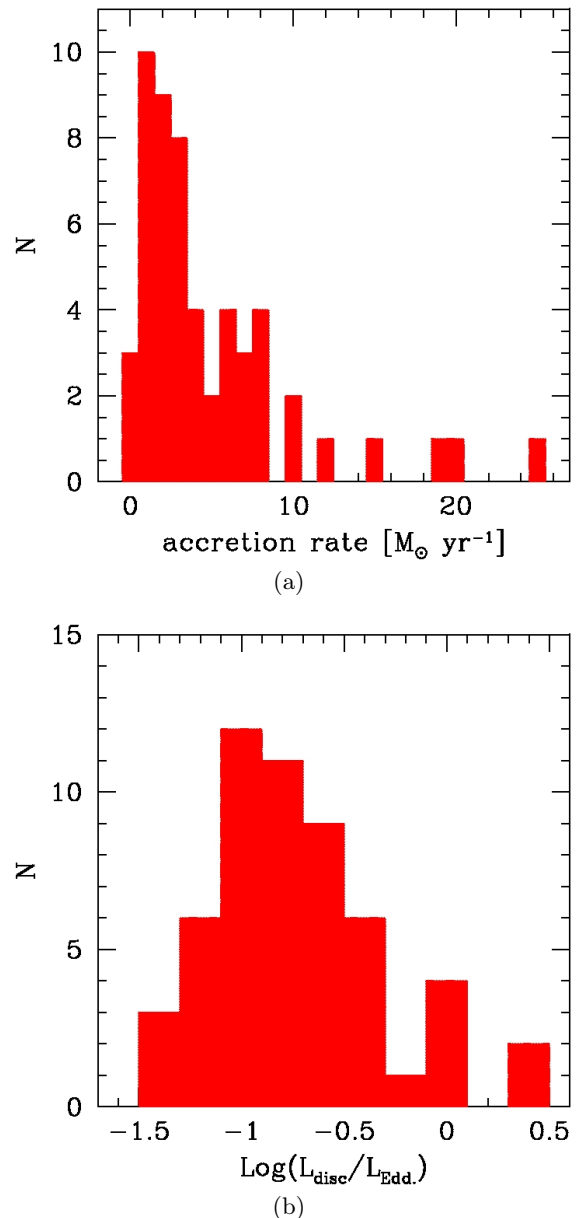


Fig. 5. Distributions of the accretion rate (top) and of the Eddington ratio (bottom) for the our FSRQs with evidence of blue bump.

implying that ultra-massive black holes associated with FSRQs must be rare.

Acknowledgements. We gratefully acknowledge very useful comments from an anonymous referee. Work supported in part by ASI/INAF agreement n. I/072/09/0 and by INAF through the PRIN 2009 ‘‘New light on the early Universe with sub-mm spectroscopy’’. This publication has made use of data products from the Wide-field Infrared Survey Explorer, which is a joint project of the University of California, Los Angeles, and the Jet Propulsion Laboratory/California Institute of Technology, funded by the National Aeronautics and Space Administration, and of the NASA/IPAC Extragalactic Database (NED) which is operated by the Jet Propulsion Laboratory, California Institute of Technology, under contract with the National Aeronautics and Space Administration.

References

- Abazajian, K., Adelman-McCarthy, J. K., Agüeros, M. A., et al. 2004, *AJ*, 128, 502
- Abdo, A. A., Ackermann, M., Ajello, M., et al. 2010, *ApJ*, 715, 429
- Ajello, M., Shaw, M. S., Romani, R. W., et al. 2012, *ApJ*, 751, 108
- Assef, R. J., Frank, S., Grier, C. J., et al. 2012, *ApJ*, 753, L2
- Blandford, R. D., & McKee, C. F. 1982, *ApJ*, 255, 419
- Bentz, M. C., Peterson, B. M., Pogge, R. W., & Vestergaard, M. 2009, *ApJ*, 694, L166
- Calderone G., Ghisellini G., Colpi M., Dotti M., 2013, *MNRAS*, 431, 210
- Cardelli, J. A., Clayton, G. C., & Mathis, J. S. 1989, *ApJ*, 345, 245
- Cash, W. 1976, *A&A*, 52, 307
- Chiaberge, M., & Marconi, A. 2011, *MNRAS*, 416, 917
- Condon, J. J., Cotton, W. D., Greisen, E. W., et al. 1998, *AJ*, 115, 1693
- Croom, S. M. 2011, *ApJ*, 736, 161
- Cutri, R.M., Wright, E.L., Conrow, T., et al. 2013, wise2.ipac.caltech.edu/docs/release/allsky/expsup/
- Decarli, R., Dotti, M., & Treves, A. 2011, *MNRAS*, 413, 39
- Donato, D., Ghisellini, G., Tagliaferri, G., & Fossati, G. 2001, *A&A*, 375, 739
- Ferrarese, L., & Ford, H. 2005, *Space Sci. Rev.*, 116, 523
- Frank, J., King, A., & Raine, D. J. 2002, *Accretion Power in Astrophysics*, by Juhan Frank and Andrew King and Derek Raine, pp. 398. ISBN 0521620538. Cambridge, UK: Cambridge University Press, February 2002
- Ghisellini, G., Della Ceca, R., Volonteri, M., et al. 2010, *MNRAS*, 405, 387
- Giommi, P., Polenta, G., Lähteenmäki, A., et al. 2012, *A&A*, 541, A160
- Gold, B., Odegard, N., Weiland, J. L., et al. 2011, *ApJS*, 192, 15
- Graham, A. W., Onken, C. A., Athanassoula, E., & Combes, F. 2011, *MNRAS*, 412, 2211
- Greene, J. E., & Ho, L. C. 2005, *ApJ*, 630, 122
- Haardt, F., & Madau, P. 2012, *ApJ*, 746, 125
- Hancock, P. J., Roberts, P., Kesteven, M. J., et al. 2011, *Experimental Astronomy*, 32, 147
- Hinshaw, G., Weiland, J. L., Hill, R. S., et al. 2009, *ApJS*, 180, 225
- Ivison, R. J., Greve, T. R., Dunlop, J. S., et al. 2007, *MNRAS*, 380, 1991
- Kaspi, S., Smith, P. S., Netzer, H., et al. 2000, *ApJ*, 533, 631
- Kaspi, S., Maoz, D., Netzer, H., et al. 2005, *ApJ*, 629, 61
- Koratkar, A. P., & Gaskell, C. M. 1991, *ApJ*, 370, L61
- Laor, A. 1990, *MNRAS*, 246, 369
- Li, L.-X., Zimmerman, E. R., Narayan, R., & McClintock, J. E. 2005, *ApJS*, 157, 335
- Malkan, M. A. 1983, *ApJ*, 268, 582
- Mannucci, F., Basile, F., Poggianti, B. M., et al. 2001, *MNRAS*, 326, 745
- Massaro, E., Giommi, P., Leto, C., et al. 2011, *Multifrequency Catalogue of Blazars (3rd Edition)*, Edited by E. Massaro, P. Giommi, C. Leto, P. Marchegiani, A. Maselli, M. Perri and S. Piranomonte. ARACNE Editrice, Rome, Italy, 118 pages
- Morrissey, P., Conrow, T., Barlow, T. A., et al. 2007, *ApJS*, 173, 682
- Netzer, H., 1990, *agn.conf...57N*
- O'Donnell, J. E. 1994, *ApJ*, 422, 158
- Onken, C. A., Ferrarese, L., Merritt, D., et al. 2004, *ApJ*, 615, 645
- Park, D., Kelly, B. C., Woo, J.-H., & Treu, T. 2012a, *ApJS*, 203, 6
- Park, D., Woo, J.-H., Treu, T., et al. 2012b, *ApJ*, 747, 30
- Planck Collaboration VII 2011, *A&A*, 536, A7
- Planck Collaboration XIII 2011, *A&A*, 536, A13
- Polletta, M., Tajer, M., Maraschi, L., et al. 2007, *ApJ*, 663, 81
- Schneider, D. P., Richards, G. T., Hall, P. B., et al. 2010, *AJ*, 139, 2360
- Shakura, N. I., & Sunyaev, R. A. 1973, *A&A*, 24, 337
- Shang, Z., Wills, B. J., Wills, D., & Brotherton, M. S. 2007, *AJ*, 134, 294
- Shankar, F., Weinberg, D. H., & Miralda-Escudé, J. 2009, *ApJ*, 690, 20
- Shaw, M. S., Romani, R. W., Cotter, G., et al. 2012, *ApJ*, 748, 49
- Shen, Y., Richards, G. T., Strauss, M. A., et al. 2011, *ApJS*, 194, 45
- Shen, Y., 2013, [arXiv:1302.2643](https://arxiv.org/abs/1302.2643)
- Trushkin, S. A. 2003, *Bulletin of the Special Astrophysics Observatory*, 55, 90
- Vestergaard, M., & Peterson, B. M. 2006, *ApJ*, 641, 689
- Wandel, A., & Petrosian, V. 1988, *ApJ*, 329, 11
- Wright, E. L., Eisenhardt, P. R. M., Mainzer, A. K., et al. 2010, *AJ*, 140, 1868
- Wu, X.-B., Wang, R., Kong, M. Z., Liu, F. K., & Han, J. L. 2004, *A&A*, 424, 793

Table 2. Best fit values of the big blue bump parameters.

WMAP ID	$\log\left(\frac{\nu_{\text{peak}}}{\text{Hz}}\right)$	$\log\left(\frac{\nu_{\text{peak}}L_{\nu}(\nu_{\text{peak}})}{\text{erg s}^{-1}}\right)$	$\log\left(\frac{L_d}{\text{erg s}^{-1}}\right)$	$\log\left(\frac{M_{\bullet}}{M_{\odot}}\right)$
9	15.52	45.62	45.90	8.53
26	15.72	46.35	46.63	8.49
27	15.29	46.00	46.26	9.18
31	15.42	46.36	46.63	9.09
39	15.32	45.37	45.64	8.80
42	15.32	45.94	46.21	9.09
89	15.42	45.32	45.59	8.57
137	15.62	46.78	47.06	8.91
150	15.33	45.81	46.07	9.01
153	15.62	46.24	46.52	8.64
155	15.39	45.81	46.08	8.88
160	15.32	46.34	46.61	9.28
166	15.32	45.69	45.96	8.96
169	15.42	45.92	46.19	8.87
173	15.42	46.49	46.77	9.17
179	15.42	45.42	45.69	8.62
182	15.57	46.05	46.33	8.64
186	15.17	46.42	46.67	9.61
190	15.15	45.72	45.96	9.30
191	15.52	46.18	46.45	8.80
195	15.39	46.10	46.37	9.04
198	15.32	45.37	45.64	8.80
203	15.52	45.21	45.48	8.32
208	15.42	46.29	46.56	9.06
221	15.52	46.28	46.56	8.86
224	15.36	45.93	46.20	8.99
228	15.32	45.40	45.67	8.81
232	15.52	45.12	45.39	8.27
236	15.32	44.95	45.21	8.58
250	15.35	45.97	46.24	9.04
265	15.67	45.72	46.00	8.28
278	15.17	45.97	46.23	9.39
284	15.62	45.70	45.97	8.36
295	15.92	46.24	46.52	8.04
306	15.62	45.44	45.71	8.23
307	15.22	45.78	46.04	9.20
310	15.42	45.75	46.02	8.79
311	15.31	46.21	46.47	9.25
316	15.38	46.36	46.63	9.19
317	15.42	44.78	45.05	8.30
327	15.71	46.46	46.74	8.58
402	15.42	45.92	46.19	8.87
407	15.82	46.74	47.02	8.49
412	15.40	46.87	47.14	9.40
415	15.37	45.24	45.51	8.63
417	15.32	46.55	46.82	9.39
428	15.39	46.34	46.61	9.14
430	15.67	46.66	46.93	8.75
434	15.42	45.94	46.21	8.88
452	15.38	46.32	46.59	9.16
455	15.32	45.87	46.14	9.05
458	15.52	45.21	45.49	8.32
462	15.37	46.11	46.38	9.07
470	15.52	46.03	46.30	8.73